Title

Reversal in the Size Dependence of Grain Rotation

Journal

Physical Review Letters, 118(9)

ISSN

0031-9007

Authors

Zhou, Xiaoling

Tamura, Nobumichi

Mi, Zhongying

et al.

Publication Date

2017-03-03

DOI

10.1103/physrevlett.118.096101

Peer reviewed

Reversal in the Size Dependence of Grain Rotation

Xiaoling Zhou,[1, 2] Nobumichi Tamura,[2] Zhongying Mi,[1] Jialin Lei,[3] Jinyuan Yan,[2] Lingkong Zhang,[1] Wen Deng,[1] Feng Ke,[1] Binbin Yue,[1] and Bin Chen[1]*

[1]Center for High Pressure Science and Technology Advanced Research, Pudong, Shanghai 201203, China

[2]Advanced Light Source, Lawrence Berkeley National Lab, Berkeley, CA 94720, USA

[3]Department of Chemistry & Biochemistry, University of California, Los Angeles, CA 90095, USA

*Corresponding author. Email: chenbin@hpstar.ac.cn

Abstract

The conventional belief, based on the Read-Shockley model for grain rotation mechanism, has been that smaller grains rotate more under stress due to the motion of the grain boundary dislocations. However, in our high-pressure synchrotron Laue x-ray micro-diffraction experiments, 70 nm nickel particles are found to rotate more than any other grain size. We infer that the reversal in the size dependence of the grain rotation arises from the crossover between the grain boundary dislocation-mediated and grain interior dislocation-mediated deformation mechanisms. The dislocation activities in the grain interiors are evidenced by the deformation texture of nickel nanocrystals. This new finding reshapes our view on the mechanism of grain rotation and helps us to better understand the plastic deformation of nanomaterials, particularly of the competing effects of grain boundary and grain interior dislocations.

Plastic deformation, a common physical process of solid materials that usually determines materials' strength, is an important scientific topic that has attracted considerable research interests in physics [1,2], planetary science [3], materials science and engineering [4-6]. Understanding plastic deformation is not only significant for fundamental science but also for various industry applications, such as making strong metals for turbine blades, making ductile ceramics for lightweight and uncooled engines, etc. General knowledge is well established for the plastic deformation of materials at the micrometer scale [7,8], whereas how plastic deformation occurs in nanocrystalline materials is still poorly understood [9], although over ten more years the constant effort of the community has yielded some encouraging achievements such as the observations of inverse Hall-Petch effects [1], twinning-induced hardness enhancement [5,6], dislocation activities in ultrafine nanocrystals [10]. Various mechanisms associated with grain boundary (GB) sliding, grain rotation, diffusion, dislocations, etc. have been proposed [11], but it is hard to really examine them well in nanoscale processes.

Grain rotation, though not usually considered to be an important mechanism of plastic deformation in bulk-sized materials, is significantly relevant in nano-mechanics [4,12,13]. For instance, oriented attachment, a grain growing path at the nanoscale, involves grain rotation [14-16]. However, the grain rotation mechanism remains elusive because several processes such as curvature-driven GB migration, lattice diffusion, dislocations, and disclinations may play roles that complicate investigations on the grain rotation mechanisms [17-19]. Based on the Read-Shockley model, the conventional belief is that GB-mediated mechanisms dominate the plastic deformation of nanomaterials, resulting in an enhancement in the grain rotation activity of fine nanocrystals [20-23], i.e. smaller grains rotate more under stress [4,15,24]. However,

computer simulations show a drop of GB mobility with decreasing grain size [25,26]. Although the observation of grain rotation in the deformation of micrometer-sized crystals is feasible [27,28], in situ probing the grain rotation of ultrafine nanocrystals is difficult, precluding further investigation of nanoscale mechanics. Whether grain rotation becomes larger or more dominant in finer nanocrystals has not yet been experimentally verified in a systematic way. In this work, we used Laue x-ray micro-diffraction to track the orientation marker in nanocrystalline media of different grain sizes and examine the size dependence of nanocrystals' grain rotation.

Since a sub-10 nm hard x-ray beam is not yet available, a practical detecting and tracking method of nanoparticle rotation had to be devised using a much larger (micron-size) x-ray beam. For good detection signals, we mixed 6~8 μm tungsten carbide (WC) particles with nickel nanoparticles (see Supplemental Material [29] for materials preparation) to mark the grain rotation magnitude of nickel nanocrystals. High pressure Laue x-ray micro-diffraction measurements were conducted at Beamline 12.3.2 of the Advanced Light Source (ALS), Lawrence Berkeley National Laboratory, USA.

In order not to lose the motion tracking of a few marker crystals embedded in a large quantity of nickel nanoparticles, we used small pressure steps and raster scanning in the experiments. A series of Laue patterns (Fig. 1) taken at each pressure step were analyzed with X-ray Micro-diffraction Analysis Software (XMAS) [32]. The most intense spots come from the diamond anvils and can be used as references to track the motion of the weaker reflections from the WC. During compression, the (10-4) and (10-5) reflections of the WC crystal shift their position with respect to the (06-2) reflection of the diamond anvils, indicating orientation changes of the tracked WC particle. During decompression, the x-ray reflections of the WC crystal shift less with respect to the bright diffraction spot of diamond. The strain changes of both the diamond anvil

and the WC crystal are also observed from the relative changes of their reflection positions at different pressures.

2D Laue micro-diffraction scans for a series of pressure steps were analyzed to generate WC crystal orientation maps (Fig. 2). Upon indexing the Laue pattern, each WC crystal is provided with an orientation matrix. Supplemental Table S1 [29] shows an example of the orientation matrices for a WC marker embedded in the 70 nm Ni nanocrystals. The rotation angle at a given pressure of the WC particle is obtained by comparing its orientation matrix with the one obtained at the first pressure step (~ 0.7 GPa). The indexation accuracy is examined with the number of indexed reflections. The number of fitted reflections varies from 0 to 13 or more (see Supplemental Material [29]). Usually, a grain with more than 8 fitted reflections is assumed to be correctly indexed. For instance, according to the orientation maps (Fig. 2), at 1.5 GPa, a WC particle embedded in the 70 nm nickel media was oriented normally to the (110) plane along the compression direction. When compressed to 4.3 GPa, the WC particle rotated to a new orientation so that its [100] direction was aligned with the compression direction. Orientation changes can be seen in the markers that were submerged in the nickel media of different particle sizes, indicating that the grain rotation occurred during compression. The different colors of the neighboring pixels reflect the polycrystalline natures of the sample aggregates. We note that as pressure increases, the automated indexing of the WC reflections becomes difficult due to the broadening of the peaks, explaining the apparent disappearance of the grains in the grain maps (Fig. 2 and Supplemental Material [29]). However, the WC markers can still be well tracked at higher pressures by manually finding and indexing the reflections.

The grain rotations of the marker crystals in nickel media are shown in Figure 3. We examined multiple grains of marker crystals for good statistics. In order to extract

the size dependence of the grain rotation, we compared the data collected at the same differential stress conditions. The differential stress of nickel medium is estimated from the data of radial X-ray diffraction experiments (see Supplemental Material [29]) at the same or close pressures. Three stages can be seen in the evolution profiles of the grain rotation. In the low pressure range (stage 1), no grain rotation occurs due to the small magnitude of applied shear (< 0.4 GPa). Whereas, in the medium pressure range (stage 2), the angle of the grain rotation increases with external shear stress. In stage 3, the grain rotation seems to have stopped under further compression, possibly due to the significantly reduced GB mobility. Although the three stage profiles look similar for the cases associated with the nickel media of different particle sizes, the stage transition pressures can be different (Fig. 3).

A surprising observation is that the marker crystals in the 70 nm nickel medium rotate more than in any other size of nickel media (Fig. 3). The grain rotation of the marker crystals may be ascribed to the following possible mechanisms: 1) the dislocation slip inside the marker crystal, and 2) the mechanical influence from the motion of the nickel media. The rotation marker, tungsten carbide, is a hard material and its yield strength was reported to be high [33]. There should not be many slips at low pressures, e.g. < 9 GPa. Even if dislocations are induced in the marker crystals, the contribution of dislocation activities to the marker crystal rotation should be similar at the same conditions of shear stress. The observed difference in the marker crystal rotation should arise from the difference in the external environment. Therefore, we infer that the rotation magnitude of the nickel nanocrystals varies with grain sizes, and under the same stress conditions nanocrystals of a certain grain size may rotate more than any other size of crystals.

Over several decades, the grain boundary dislocation mechanism was proposed and widely accepted to describe and understand grain rotations [34,35]. It has already been established in theoretical [36,37], computer simulation [38] and experimental studies [4,39] that under shear stresses grain rotation occurs due to dislocation displacement at grain boundaries. In the case of applied stress, the structure of a grain boundary can be basically described as an arrangement of dislocations with a mixed edge-screw character [35]. The Burgers vector of such dislocations has an edge and two screw components, which are directed normal to the boundary plane and within the boundary plane, respectively. Due to the edge component, the dislocation can move along the normal to the grain boundary plane and hence produces a shear. The concurrent displacement of the two screw components in the same direction causes two additional perpendicular shears, generating a rotation confined to the region traversed by the boundary. Consequently, all the screw components experience a Peach-Koehler force parallel to the boundary plane and their motion at the grain boundary gives rise to a rotation of the adjacent grains relative to each other, i.e. misorientation changes across the boundary. In previous simulations [18,24], the grain boundary dislocation mechanism was reported to yield a d^{-n} dependence of rotation rate, where d is the grain size and the index n is variously 2, 3, 4 or 5, depending on the rotation mechanism assumed in the theory. In other words, grain rotation is believed to be more active in finer nanocrystals.

With those conventional theories, it is difficult to interpret the observed maximal grain rotation of the nanocrystals at a certain particle size. We speculate that the plastic deformation in the grains' interior is also relevant. Nanocrystals are usually thought to be nearly defect-free. The dislocations in the grain interior are not considered in conventional grain rotation theories [24,40], mainly because there was no experimental

evidence to support the grain shearing models in which dislocations glide across the nano grains [18,41]. However, the updated finding that grain interior dislocations are still active in nano crystals down to 3 nm [10] provides a reasonable interpretation and supporting evidence for the observed size dependence of grain rotation in this study. Deformation texture is considered to form as a consequence of the activity of the slip system inside materials and hence it can be used to check the slip activities in the grain interior [10,42]. For a complete comparison, we took texture measurements, similar as those reported in Ref. [10], for more sizes of nickel samples. Details about the texture measurements at Beamline 12.2.2 of ALS can be found in Supplemental Material [29].

As shown in the unrolled radial diffraction images collected at 10 -11 GPa (Fig. 4, top), variations in the diffraction peak position with respect to the compression direction can be clearly seen, indicating differential stresses in the material. They also display systematic intensity variations that can be used to deduce texture. At 10 GPa, strong diffraction intensity variations are seen in the 70 and 500 nm nickel. More modest but resolvable intensity variations are observed in the 20 and 40 nm nickel and there is no apparent intensity variations observed in the 3 nm nickel around 11 GPa. The observed textures (Fig. 4, bottom) in nano grains indicate that grain interior dislocations still exist in nanocrystals but tend to be weak with decreasing grain size.

The physics picture looks like this: grain interior and boundary dislocations compete in influencing the grain rotations of nanocrystals under external stresses. The texture strength decreases with the particle size, indicating that the contribution from the grain interior dislocations decreases with the decreasing particle size, while the grain boundary dislocations tend to be more operative in smaller grains, as suggested in earlier studies [4,24]. The two opposite trends in the particle size-dependence of the grain rotation result in the maximal grain rotation of certain sized nanocrystals. The

mechanism crossover is supported by the texture measurements of this study and previous observations on grain boundary migration and grain rotation [4,10,12,18]. We realize that the role of grain interior dislocations in plastic deformation of nanocrystals was seriously overlooked before. Our experimental observations indicate that stresses in nanocrystalline materials induce dislocations and considerably affect the plastic properties, and hence the strength and ductility of materials. The competing effects could result in enhanced mechanical properties at a critical particle size, and this would provide guidance in materials production and application. Specifically on grain rotation mechanisms, the Read-Shockley-model-based theories should be revised to include the contributions of grain interior dislocations. The knowledge on the size dependence of grain rotation would help us to better design crystal growth or materials with special mechanical properties.

Admittedly, the indirect measurements of grain rotation in this study may contain some degree of uncertainty in the tracking accuracy of trend change. Due to the technical limitations, at this stage we cannot devise a better approach than using a marker. Inaccuracy in the determination of the critical particle size of the mechanism crossover may exist. In the future with advanced techniques, such as sub-10 nm XRD combined with 3D nano tomography techniques or high-pressure TEM, more accurate measurements may give that the reversal occurs at 59 nm or 81 nm. But we think that the physics behind would not change much. The reversal itself is more important than where it is, because the trend or trend change of a physical behavior usually hints physics behind.

In this letter, we report the reversal in the grain rotation of nanocrystals and correlate the new observation with previous results for making a physics picture behind. Just from previous observations on dislocation activities in ultrafine (down to 3 nm)

nickel nanocrystals [10], at most, we can only say that grain rotation could be affected somehow because grain interior dislocations may play a role. The reproducible Laue micro-XRD measurements reveal a turnover in the size dependence of grain rotation, suggesting that the change in the grain rotation of the marker can reflect the difference in the mechanical influence from the nickel media. This observation really reshapes our view on the mechanism of grain rotation at the nanoscale. This finding prompts the revision of the Read-Shockley model for including the competing effects from grain interior and boundary dislocations in nanocrystals. The plastic deformation of nanocrystals, particularly of grain interior dislocation associated processes, should be re-examined carefully, better in-situ at the conditions of stress, and consequently, more correct knowledge and proper guidance to designing and engineering materials' properties, functionalities and processing, such as nanoalloying, crystal growth, nanocatalysis, nanomedicine, etc. can be expected.

X. Z. thanks Haini Dong for DAC technique training, Yanping Yang for SEM measurements, Hongwei Sheng, Hengzhong Zhang, Jiuhua Chen, Raymond Jeanloz, and Ho-Kwang Mao for useful discussions and comments. The authors acknowledge the support of NSAF (Grant No：U1530402). X. Z. was partially supported by the ALS Doctoral Fellowship in Residence Program. The Advanced Light Source is supported by the Director, Office of Science, Office of Basic Energy Sciences, Materials Sciences Division, of the U.S. Department of Energy under Contract No. DE-AC02-05CH11231 at Lawrence Berkeley National Laboratory and University of California, Berkeley, California.

[1] J. Schiøtz, F. D. D. Tolla, and K. W. Jacobsen, Nature **391**, 561 (1998).

[2] M. Jo, Y. M. Koo, B.-J. Lee, B. Johansson, L. Vitos, and S. K. Kwon, Proc. Natl. Acad. Sci. **111**, 6560 (2014).

[3] S. Merkel, A. Kubo, L. Miyagi, S. Speziale, T. S. Duffy, H.-k. Mao, and H.-R. Wenk, Science **311**, 644 (2006).

[4] L. Wang, J. Teng, P. Liu, A. Hirata, E. Ma, Z. Zhang, M. Chen, and X. Han, Nat Commun **5**, 4402 (2014).

[5] L. Lu, X. Chen, X. Huang, and K. Lu, Science **323**, 607 (2009).

[6] Q. Huang *et al.*, Nature **510**, 250 (2014).

[7] J. P. Hirth and J. Lothe, *Theory of Dislocations*, (Kreiger Publishing, UK, Malabar, 1992).

[8] W. J. Clegg, Science **286**, 1097 (1999).

[9] S. Yip, Nature **391**, 532 (1998).

[10] B. Chen *et al.*, Science **338**, 1448 (2012).

[11] J. Weissmüller and J. Markmann, Adv. Eng. Mater. **7**, 202 (2005).

[12] M. Dao, L. Lu, R. Asaro, J. Dehosson, and E. Ma, Acta Mater. **55**, 4041 (2007).

[13] I. A. Ovid'ko and A. G. Sheinerman, Appl. Phys. Lett. **98**, 181909 (2011).

[14] R. L. Penn and J. F. Banfield, Science **281**, 969 (1998).

[15] D. Moldovan, V. Yamakov, D. Wolf, and S. R. Phillpot, Phys. Rev. Lett. **89**, 206101 (2002).

[16] D. Tan, W. Zhou, W. Ouyang, Z. Mi, L. Kong, W. Xiao, K. Zhu, and B. Chen, Cryst. Eng. Comm. **16**, 1579 (2014).

[17] I. Zizak, N. Darowski, S. Klaumunzer, G. Schumacher, J. W. Gerlach, and W. Assmann, Phys. Rev. Lett. **101**, 065503 (2008).

[18] K. E. Harris, V. V. Singh, and A. H. King, Acta Mater. **46**, 2623 (1998).

[19] M. Murayama, J. M. Howe, H. Hidaka, and S. Takaki, Science **295**, 2433 (2002).

[20] Z. Shan, E. A. Stach, J. M. Wiezorek, J. A. Knapp, D. M. Follstaedt, and S. X. Mao, Science **305**, 654 (2004).

[21] J. F. Banfield, S. A. Welch, H. Zhang, T. T. Ebert, and R. L. Penn, Science **289**, 751 (2000).

[22] A. Alivisatos, Science **289**, 736 (2000).

[23] B. Chen, K. Lutker, J. Lei, J. Yan, S. Yang, and H. K. Mao, Proc. Natl. Acad. Sci. **111**, 3350 (2014).

[24] M. Upmanyu, D. J. Srolovitz, A. E. Lobkovsky, J. A. Warren, and W. C. Carter, Acta Mater. **54**, 1707 (2006).

[25] D. Farkas, S. Mohanty, and J. Monk, Phys. Rev. Lett. **98**, 165502 (2007).

[26] M. Y. Gutkin and I. Ovid'Ko, Appl. Phys. Lett. **87**, 251916 (2005).

[27] L. Margulies, G. Winther, and H. F. Poulsen, Science **291**, 2392 (2001).

[28] B. Jakobsen, H. F. Poulsen, U. Lienert, J. Almer, S. D. Shastri, H. O. Sørensen, C. Gundlach, and W. Pantleon, Science **312**, 889 (2006).

[29] See Supplemental Materials at xxx which includes Refs. [30-31], for Materials preparation, experimental details, calculations of the rotation angle and estimations of differential stress.

[30] A. P. Hammersley, FIT2D: An Introduction and Overview (ESRF Internal Report, ESRF97HA02T, 1997).

[31] A. K. Singh, C. Balasingh, H.-k. Mao, R. J. Hemley, and J. Shu, J. Appl. Phys. **83**, 7567 (1998).

[32] N. Tamura, XMAS: a versatile tool for analyzing synchrotron X-ray microdiffraction data, in *Strain and Dislocation Gradients from Diffraction. Spatially Resolved Local Structure and Defects*, (Imperial College Press, London, 2014).

[33] A. L. Ruoff and J. Wanagel, J. Appl. Phys. **46**, 4647 (1975).

[34] J. C. M. Li, J. Appl. Phys. **33**, 2958 (1962).

[35] T. Gorkaya, K. D. Molodov, D. A. Molodov, and G. Gottstein, Acta Mater. **59**, 5674 (2011).

[36] W. T. Read and W. Shockley, Phys. Rev. **78**, 275 (1950).

[37] J. W. Cahn, Y. Mishin, and A. Suzuki, Acta Mater. **54**, 4953 (2006).

[38] V. A. Ivanov and Y. Mishin, Physical Review B **78** (2008).

[39] T. Gorkaya, D. A. Molodov, and G. Gottstein, Acta Mater. **57**, 5396 (2009).

[40] R. Kobayashi, J. A. Warren, and W. C. Carter, Physica D: Nonlinear Phenomena **140**, 141 (2000).

[41] A. H. King and K. E. Harris, in *Proceedings of the 2nd international conference on grain growth in polycrystalline materials* Kitakyushu, Japan, 1996).

[42] R. Cahn, Philosophical Transactions of the Royal Society of London A: Mathematical, Physical and Engineering Sciences **288**, 159 (1978).

Figure Captions:

FIG. 1. Representative pattern of Laue XRD measurements (left) and close-up views on the pressure evolutions of two Laue spots [(10-4) and (10-5)] of a marker-grain (right). The centroid coordinates of all cut-offs are 548 and 355 with a zoom factor of 3.

FIG. 2. 2D orientation maps of WC markers embedded in the nickel media. The vertical and horizontal axes correspond to the 2D scanning directions of sample stage. Different colors on the maps indicate different crystalline orientations, as referenced in the color triangle on the right. The numbers at the top right corners are pressure in units of GPa.

FIG. 3. Rotation angles of marker grains. (a) as a function of the lattice parameter ratio *c*/*a* of the WC crystals, equivalently, of differential stress of nickel media; (b) and (c), as the logarithmic functions of the nickel medium grain-size at the same *c*/*a* level. The differential stress of the nickel medium is estimated from the radial X-ray diffraction experiments. The correlation between *c/a* of WC crystal and differential stress is established by comparing the data from radial DAC XRD and Laue micro-XRD measurements of nonhydrostatically compressed samples. The closed and open symbols represent the data collected in compression and decompression cycles, respectively. "GB⊥" and "GI⊥" in (b) and (c) represent the grain boundary and grain interior dislocations, respectively. The rotation angles for plot (**b)** and (**c)** are the average of several measurements near the selected differential stress. The ellipses in (a) and the lines connecting the data points in (b) and (c) are guides for the eye. The transition of WC markers from stage 2 to stage 3 occurs around 0.6 GPa for 500 nm,

0.8 GPa for 3 nm and 200 nm, and 1.3 GPa for 20 nm, 40 nm, 70 nm media, respectively.

FIG. 4. Top: Azimuthally (0~360^{o}) unrolled diffraction images of nickel. Bottom: Inverse pole figures of nickel along the compression direction (normal direction); (a) 3 nm; (b) 20 nm; (c) 40 nm; (d) 70 nm; (e) 500 nm. The long and short black arrows represent the maximum and minimum compression direction, respectively. All diffractions were measured with an x-ray wavelength of 0.4959 Å. Equal area projection and a linear scale are used. Texture strength is expressed as multiples of the random distribution (m.r.d.), where m.r.d. = 1 denotes random distribution and a higher m.r.d. number represents a stronger texture. A weak texture was observed in 3 nm nickel above 18.5 GPa [10].

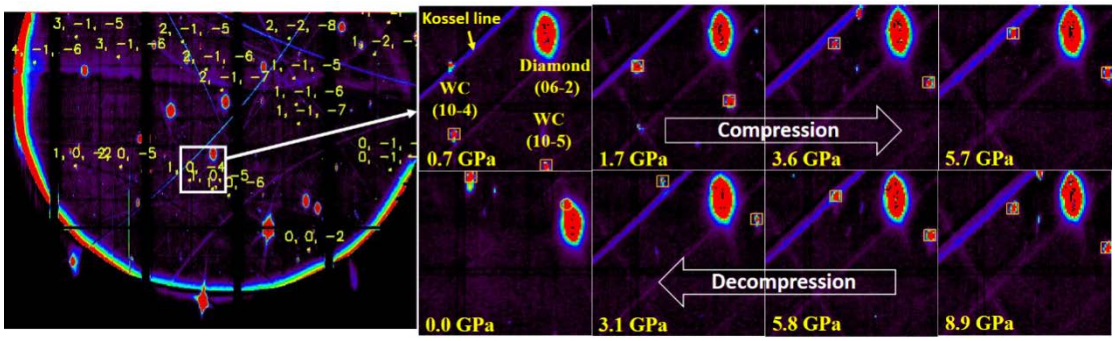
Kossel line
Diamond
(06-2)
WC
(10-4)
WC
(10-5)
0.7 GPa
1.7 GPa
3.6 GPa
5.7 GPa
Compression
Decompression
0.0 GPa
3.1 GPa
5.8 GPa
8.9 GPa

Figure 1

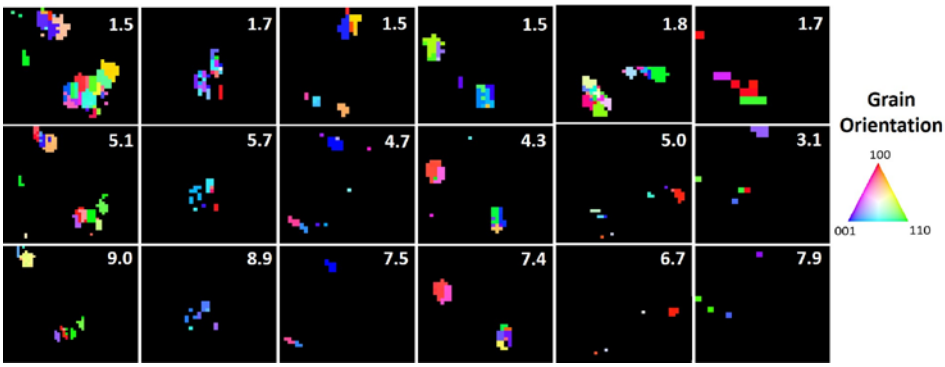
1.5
1.7
1.5
1.5
1.8
1.7
5.1
5.7
4.7
4.3
5.0
3.1
9.0
8.9
7.5
7.4
6.7
7.9
Grain Orientation
100
001
110

Figure 2

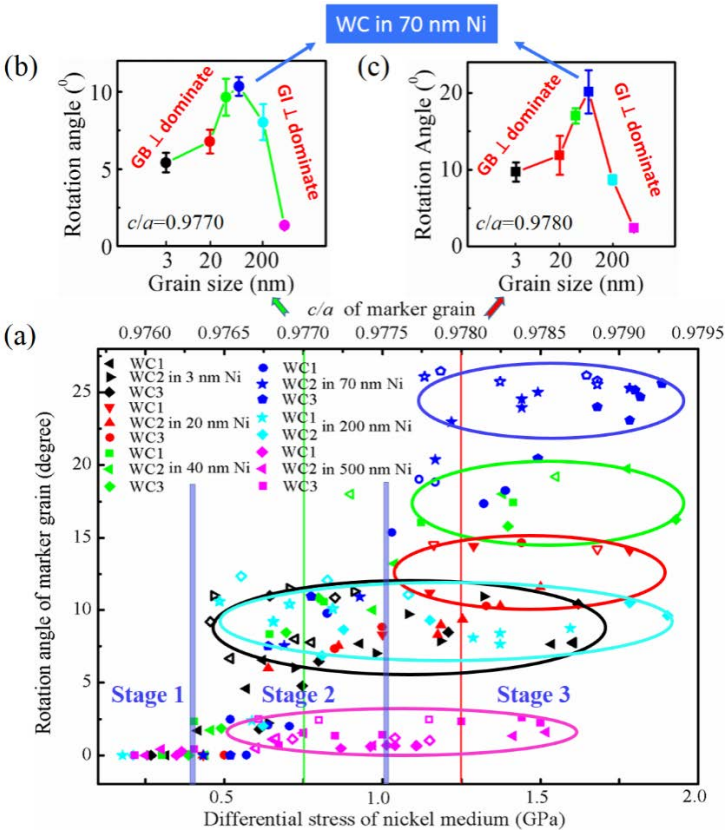
WC in 70 nm Ni
(b)
(c)
Rotation angle (°)
Rotation Angle (°)
GB ⊥ dominate
GI ⊥ dominate
c/a=0.9770
c/a=0.9780
Grain size (nm)
c/a of marker grain
(a)
Rotation angle of marker grain (degree)
Differential stress of nickel medium (GPa)
Stage 1
Stage 2
Stage 3
WC1
WC2 in 3 nm Ni
WC3
WC2 in 20 nm Ni
WC2 in 40 nm Ni
WC2 in 70 nm Ni
WC2 in 200 nm Ni
WC2 in 500 nm Ni

Figure 3

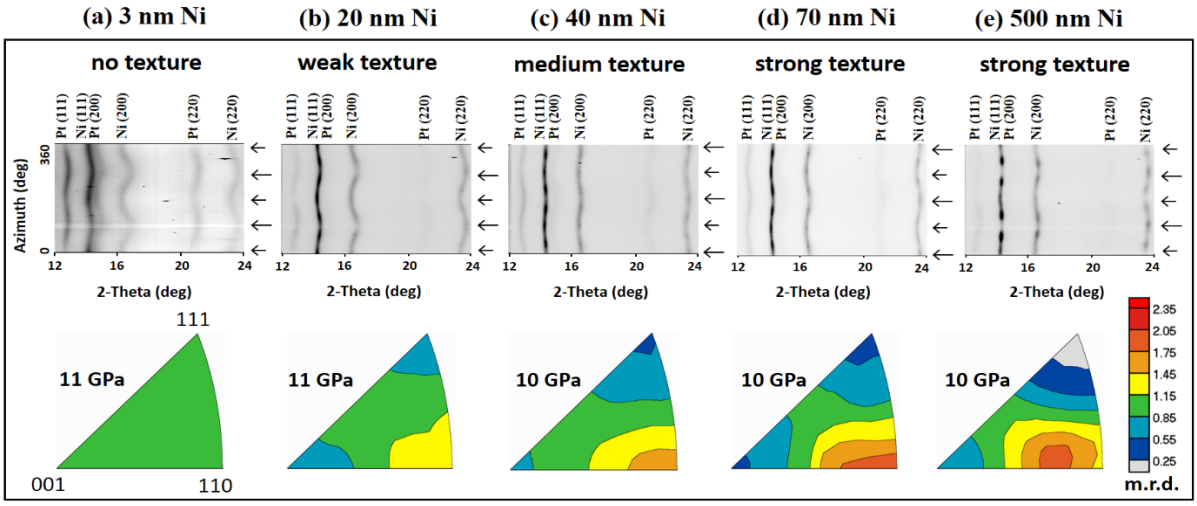
(a) 3 nm Ni
(b) 20 nm Ni
(c) 40 nm Ni
(d) 70 nm Ni
(e) 500 nm Ni
no texture
weak texture
medium texture
strong texture
strong texture
Pt (111)
Ni (111)
Pt (200)
Ni (200)
Pt (220)
Ni (220)
Azimuth (deg)
360
0
12
16
20
24
2-Theta (deg)
111
11 GPa
11 GPa
10 GPa
10 GPa
10 GPa
001
110
2.35
2.05
1.75
1.45
1.15
0.85
0.55
0.25
m.r.d.

Figure 4